TÜBİTAK

Turkish Journal of Physics

http://journals.tubitak.gov.tr/physics/

Research Article

Turk J Phys
(2019) 43: 481 – 492
© TÜBİTAK
doi:10.3906/fiz-1905-2

The behaviour of the diamagnetic current modified MRI in different rotation profiles

Suzan DOĞAN*

Department of Astronomy and Space Sciences, Faculty of Science, University of Ege, 35100, Bornova, İzmir, Turkey

Received: 02.05.2019 • **Accepted/Published Online:** 20.08.2019 • **Final Version:** 21.10.2019

Abstract: Magnetohydrodynamic turbulence driven by magnetorotational instability (MRI) has been widely accepted as an efficient mechanism for transporting angular momentum radially outward in the discs. Previously, we have shown the triggering effect of the magnetization currents and the gradients produced by these currents on MRI for Keplerian discs. In this work, we examine the properties of the diamagnetic current modified MRI for the discs where the epicyclic frequencies deviate from Keplerian behaviour. We show that the diamagnetic effect modifies the instability both for an increasing and for a decreasing angular momentum with radius. The novel unstable region produced by magnetization effects still exists even if $d\Omega^2/d\mathrm{R} > 0$, where $\Omega(\mathrm{R})$ is the angular velocity. Inclusion of the diamagnetic effect increases the maximum dimensionless growth rate $\mathrm{s}_m = 0.25$ which was found from the classical MRI to $\mathrm{s}_m = 0.59$ for an outwardly increasing angular velocity profile with $\kappa^2 > 4\Omega^2$, where κ is the epicyclic frequency. Moreover, the maximum dimensionless growth rate is obtained as $\mathrm{s}_m = 8.58$ for a an outwardly decreasing angular velocity profile with $0 < \kappa^2 < \Omega^2$. Decreasing the magnetic field strength which is already weak, leads to more rapid growth in any differential rotation profile.

Key words: accretion discs, instabilities, plasma, magnetohydrodynamics

1. Introduction

The global stability of axisymmetric flows in a vertical magnetic field was first studied by [1] and [2]. In these investigations, it was shown that the flow becomes unstable in the presence of a vanishingly weak field. The importance of these findings in the context of accretion disc dynamics was pointed out by [3], and since then, this unstable behaviour, which is now called the magnetorotational instability (MRI), has been extensively studied in many astrophysical environments. In the non-linear regime, MRI rapidly generates magnetohydrodynamic (MHD) turbulence which has been widely accepted as an efficient process for the angular momentum transport in accretion discs, e.g. [4 – 7].

[3] showed the destabilization of the flow by a weak magnetic field frozen into the disc fluid with a Keplerian rotation. The authors found no instability for a disc with an outwardly increasing angular velocity curve (where the epicyclic frequency is $\kappa^2 = 5\Omega^2$). Later, the effects of different rotation profiles on MRI have been considered in several investigations. [8] examines the behaviour of the instability under very general circumstances, and claim their results are also applicable to non-Keplerian 'thick' discs. Furthermore, [9] who investigated the effects of Hall electromotive forces (HEMFs) on the MRI, show that the inclusion of the

*Correspondence: suzan.dogan@ege.edu.tr

This work is licensed under a Creative Commons Attribution 4.0 International License.

HEMFs lead to instability in any rotation profile. The HEMFs destabilize the flows even those with outwardly increasing angular velocity. When the Hall effect is ignored, the classical MRI requires $d\Omega^2/dR < 0$. However, the inclusion of the Hall currents changes the instability criterion into $d\Omega^2/dR \neq 0$. Because negative $Y = (\mathrm{k}\nu_H/\Omega)^2$ parameter becomes possible with the inclusion of the Hall effect, and this allows $X = (\mathrm{k}\nu_A/\Omega)^2$ parameter to have positive values, even if $d\Omega^2/dR > 0$. Here, ν_H is the Hall velocity, defined by $\nu_H^2 = \Omega.\mathbf{B}c/2\pi e\mathrm{n}_e$ and ν_A is the Alfvén velocity, defined by $\nu_A^2 = B^2/4\pi\rho$,k is the wavenumber, Ω is the local angular velocity vector of the disc, $\mathbf{B}$ is the magnetic field, e is the magnitude of the electron charge, n_e is the electron number density, $\rho$is the mass density. For a disc with an outwardly increasing velocity profile, e.g. $\kappa^2 = 5\Omega^2$, they find that the Y < 0 regions can be unstable. Thus, any differential rotation profile has the potential to become unstable. On the other hand, [10] examines the properties of stable and unstable modes for various rotation profiles. They investigate several cases where the angular momentum and angular velocity of the disc fluid either increasing ($\kappa^2 > 4\Omega^2$) or decreasing ($\kappa^2 < 0$) in radial direction, and where the angular momentum is constant ($\kappa^2 = 0$). They conclude that the classical case with a radially decreasing angular momentum produces a stable MRI mode and an unstable Rayleigh mode. Conversely, if the angular momentum increases radially outward, an unstable MRI mode appears at small wavenumbers.

[11] and [12] extended the analysis of [9] including the magnetization effects. Magnetization is the quantity of magnetic moment ($\mu = mv_\perp^2/2B$, where m is the mass of the particle, $v_\perp$ is its velocity prependicular to the magnetic field) per unit volume, and it is inversely proportional to the magnetic field strength. Thus, the diamagnetic effects are expected to become important in flows where the field strength is low. A weak field is needed for MRI, and the diamagnetic effect makes the field even weaker. This weakening effect yields a novel unstable mode, and moreover, the maximum value of the growth rate becomes higher than the Oort A-value [11 – 12].

In the presence of diamagnetism, magnetization currents give rise to a gradient both in the magnetic field and in the perpendicular component of the velocity. [11] performed their analysis by neglecting the gradient in perpendicular velocity. In [12], we included both of these gradients in our analysis, and found that the instability has become more powerful. Diamagnetism has a destabilizing effect in addition to whistlers. Both investigations restricted their analysis to Keplerian discs. When the disc is Keplerian, the epicyclic and the orbital frequencies are nearly equal, i.e. $\kappa^2 \approx \Omega^2$. However, the epicyclic frequency of the fluid element may deviate from the Keplerian behaviour through several effects. There are several circumstances where κ^2 differ from Ω^2, especially in the inner regions of discs around Kerr black holes [13] or discs in binary systems, i.e. the inner (outer) parts of circumbinary (circumprimary) discs due to the tidal torques, e.g. [14 – 15]. Discs with significant internal pressure also have non-Keplerian angular momentum distributions [13]. The local angular velocity is also expected to differ significantly from its Keplerian value in the boundary layer around an accreting star, the region of the disc in which the angular velocity has an outwardly increasing profile ($d\Omega$ / dR > 0), e.g. [16]. Furthermore, any magnetic field threading the disc can lead to a deviation of rotation from Keplerian. Particularly, in the presence of magnetization currents, gradients in the magnetic field strengh and the perpendicular component of the velocity may change the rotation profile locally (see Section 2). Thus, we aim to apply our analysis to different laws of differential rotation.

Bearing the destabilizing role of the diamagnetic effects in mind, we extend our stability analysis [12] where we included the magnetization effects on MRI to different rotation profiles. The paper is structured as

follows: In Section 2, we summarize the mathematical formalism of diamagnetic currents, describe the governing MHD equations with their assumptions, and derive the dispersion relation. In Section 3, we provide the growth rates of the instability. Finally, in Section 4, we present our conclusions.

2. Preliminaries

2.1. Diamagnetism

We investigate the linear stability of a disc at a fiducial radius where both Hall currents and the magnetization currents are present. The diamagnetic effect emerges when particles gyrating in an external magnetic field produce their own dipole magnetic field. If we assume that the charged particles gyrating around the field lines create a net current at the boundary of a closed circuit, this current, in turn, will produce an additional magnetic field the direction of which is the same as the external magnetic field outside the circuit, and the opposite within the circuit. Thus, the net magnetic field inside this region will become weaker than that outside. The decrease (increase) in the magnetic field strength within (outside) the circuit will produce a gradient in the radial direction.

If the local currents are persistent enough to create a magnetic field gradient in the disc, electrons and ions experience a magnetic pressure. The magnetic pressure force pushes the frozen-in particles into the region within the current, and dragging of the frozen-in particles bend the magnetic field lines. Particles in a magnetic field with a gradient and curvature acquire a drift velocity and set in a cycloid orbit. In their cycloid trajectory, particles encounter weak and strong magnetic fields. If the magnetic moment $\left(\mu = mv_{\perp}^{2}/2B\right)$ is conserved, the perpendicular velocity of the particles also vary depending on the magnetic field strength. Particle's velocity at the top of the cycloid trajectory where the Larmor radius is smaller will be higher than the velocity at the bottom. This brings about a gradient both to the radial and to the azimuthal components of the velocity.

The local counterfield produced by the charged particles can be obtained by integrating the magnetic moment for all the charged particles in a unit volume [17]

$$\mathbf{M} = \int_{4\pi} \int_{0}^{\infty} N\left(E,\,\theta\right) \mu\left(E,\,\theta\right) dE d\theta \tag{1}$$

where $N(E,\theta)\, dEd\Omega$ is the number density of charged particles having velocity within $d\Omega$ around pitch angle θ and energy within dE around E. Using the definition of the magnetic moment, the magnetization is found as [17 – 18]

$$\mathbf{M} = -\frac{2\mathbf{B}}{3B^{2}} W_{k} \tag{2}$$

where $W_k = nmv_{\perp}^{2}/2$ is the kinetic energy density. We assume that the global magnetic field value in the absence of any magnetization effects is $\boldsymbol{H}$. Thus, in the presence of magnetization, the net magnetic field in the close neighborhood of the magnetization current is

$$\mathbf{B} = \mathbf{H} + 4\pi\mathbf{M} = \mathbf{H} - \frac{8\pi}{3}\frac{\mathbf{B}}{B^{2}} W_{k} = \mathbf{H} - \frac{1}{3}\frac{W_{k}}{W_{B}}\mathbf{B} = \mathbf{H} - \varepsilon\mathbf{B} \tag{3}$$

where $W_B = B^2/8\pi$ is the magnetic field energy density, $\varepsilon = W_k \,/\, 3W_B$ is the 'magnetization parameter'. The total current density is

$$\mathbf{J} = \mathbf{J}_{\text{ext}} + \mathbf{J}_{\text{mag}} = \frac{c}{4\pi}\nabla \times \mathbf{H} + c\nabla \times \mathbf{M} = \frac{c}{4\pi}\nabla \times \mathbf{H} - c\nabla \times \frac{2W_{k}}{3B^{2}}\mathbf{B} \tag{4}$$

The vector operations give the total current density in terms of magnetic field gradient and the resulting perpendicular velocity gradient as

$$\mathbf{J} = \frac{c}{4\pi}\left[(1-\varepsilon)\right]\nabla\times\mathbf{B}+2\varepsilon\frac{\nabla B}{B}\times\mathbf{B}-2\varepsilon\frac{\nabla v_{\perp}}{v_{\perp}}\times\mathbf{B} \tag{5}$$

[11]. As mentioned before, [11] ignored the gradient in perpendicular velocity by dropping the term containing $\nabla v_{\perp}$ in Eq. (5). Then, [12] included the $\nabla v_{\perp}$ term in their investigation for Keplerian discs, i.e. $\kappa = \Omega$. Here, we shall follow the same analysis, but generalize their investigation for the discs/disc regions where the epicyclic frequency deviate from Keplerian behaviour. Therefore, we shall consider the cases with $\kappa \neq \Omega$. Other than that, the basic equations will remain the same.

2.2. MHD Equations and the Dispersion Relation

The fundamental dynamical equations are mass conversation,

$$\frac{\partial\rho}{\partial t} + \nabla\cdot(\rho\nu) = 0, \tag{6}$$

the equation of motion,

$$\rho\frac{\partial\nu}{\partial t} + (\rho\nu\cdot\nabla)\,\nu = -\nabla P+\frac{1}{c}\mathbf{J}\times\mathbf{B}, \tag{7}$$

and the induction equation,

$$\frac{\partial\mathbf{B}}{\partial t} = \nabla\times\left[\nu\times\mathbf{B}-\eta\frac{4\pi}{c}\mathbf{J}-\frac{\mathbf{J}\times\mathbf{B}}{en_e}\right]. \tag{8}$$

Here ν is the fluid velocity, η is the microscopic resistivity, and n_e is the electron number density. In Eqns. (7) and (8), the current density is given by

$$\mathbf{J} = \frac{c}{4\pi}\nabla\times\mathbf{B}. \tag{9}$$

We investigate the local stability of a disc threaded by a vertical magnetic field with a gradient in the radial direction, i.e. $\mathbf{B} = B(R)\hat{z}$. Thus, we can write the gradient of the magnetic field as $\nabla B = (dB/dR)\,\hat{R}$ The disc fluid's bulk velocity is in the azimuthal direction and, magnetic pressure and the magnetic tension force restrict the disc fluid's motion in the radial direction. Therefore, we assume that the gradient of the perpendicular velocity is in the radial direction, i.e. $\nabla v_{\perp} = (dv_{\perp}/dR)\,\hat{R}$.

We shall use the Boussinesq approximation, and thus assume that $\nabla\cdot\nu = 0$. We should note that the velocity field of the disc fluid is nearly but not exactly incompressible [8]. We shall work in standard cylindrical coordinates $(R,\ \phi,\ z)$ with the origin at the disc center. To keep the coefficients of the dispersion relation real, we assume that the perturbations are proportional to $\exp(\mathrm{i}kz+\omega t)$ where k is the wavenumber perpendicular to the disc and ω is the wave frequency. Therefore, if any of the solutions has a positive real part, i.e. $\mathcal{R}\ [\omega] > 0$, we expect to see an exponential growth in perturbations with time. Under these assumptions, we obtain the linearized radial, azimuthal, and vertical components of Eqn. (7) as follows:

$$\omega\delta\nu_R - 2\Omega\delta\nu_{\phi} - (1-\varepsilon)\,\frac{ik}{4\pi\rho}B\delta B_R + \frac{1}{4\pi\rho}\left[(1+3\varepsilon)\,\nabla B - 4\varepsilon B\frac{\nabla\Omega}{\Omega}\right]\delta B_z = 0 \tag{10}$$

$$\omega\delta\nu_\phi + \frac{\kappa^2}{2\Omega}\delta\nu_R - (1-\varepsilon)\frac{ik}{4\pi\rho}B\delta B_\phi = 0 \tag{11}$$

$$ik\frac{\delta P}{\rho} - \frac{1}{4\pi\rho}\left[(1+\varepsilon)\nabla B - 2\varepsilon B\frac{\nabla\Omega}{\Omega}\right]\delta B_R = 0 \tag{12}$$

where the epicyclic frequency is defined as $\kappa^2 = 4\Omega^2 + d\,\Omega^2/d\,\ln\,R$. Similarly, we find the linearized components of Eqn. (8) as follows:

$$ikB\delta\nu_R - \left[\omega + (1-\varepsilon)k^2\eta\right]\delta B_R - (1-\varepsilon)\frac{c}{4\pi en_e}k^2B\delta B_\phi = 0 \tag{13}$$

$$\begin{aligned}&\left[\frac{c}{4\pi en_e}\left((1-\varepsilon)k^2B + (1+\varepsilon)\nabla^2B - 2\varepsilon\left(B\frac{\nabla^2\Omega}{\Omega} + \nabla B\frac{\nabla\Omega}{\Omega} - B\left(\frac{\nabla\Omega}{\Omega}\right)^2\right)\right) + \frac{d\Omega}{d\ln R}\right]\delta B_R\\ &-\left[\omega + (1-\varepsilon)k^2\eta - 2\varepsilon\eta\left(\frac{\nabla^2B}{B} - \left(\frac{\nabla B}{B}\right)^2 - \frac{\nabla^2\Omega}{\Omega} - \left(\frac{\nabla\Omega}{\Omega}\right)^2\right)\right]\delta B_\phi\\ &+ikB\delta\nu_\phi + \frac{c}{4\pi en_e}2\varepsilon\left(ik\nabla B - ikB\frac{\nabla\Omega}{\Omega}\right)\delta B_z = 0\end{aligned} \tag{14}$$

$$\begin{aligned}&\nabla B\delta\nu_R + 2\varepsilon\eta ikB\frac{\nabla\Omega}{\Omega}\delta\nu_\phi - \left[\omega + (1-\varepsilon)k^2\eta + 2\varepsilon\eta\left(ik\frac{\nabla B}{B} - \frac{\nabla^2B}{B} + \left(\frac{\nabla B}{B}\right)^2 - \frac{\nabla^2\Omega}{\Omega} + \left(\frac{\nabla\Omega}{\Omega}\right)^2\right)\right]\delta B_z\\ &-\frac{c}{4\pi en_e}\left[(1+\varepsilon)ik\nabla B - 2\varepsilon ikB\frac{\nabla\Omega}{\Omega}\right]\delta B_\phi = 0\end{aligned} \tag{15}$$

In the limit of zero resistivity, eqns. (10 - 15) yield a quartic dispersion relation

$$\begin{aligned}&s^4 + s^2\left\{\begin{array}{l}\tilde\kappa^2 + 2X(1-\varepsilon) + \frac{Y}{4}(1-\varepsilon)\left[Y(1-\varepsilon) + \frac{d\ln\Omega^2}{d\ln R}\right] + \left(\frac{d\ln B}{d\ln R}\right)^2 M_A^{-2}\left[(1+3\varepsilon) - \chi Y\varepsilon(1+\varepsilon)\right]\\ +\frac{3}{4}\frac{d\ln B}{d\ln R}\left(\frac{d\ln\Omega^2}{d\ln R}\right)_{MC}M_A^{-2}\chi Y\varepsilon(1+3\varepsilon) + \frac{1}{8}\left(\frac{d\ln\Omega^2}{d\ln R}\right)^2_{MC}M_A^{-2}\chi Y\varepsilon(8-9\varepsilon)\end{array}\right\}\\ &+\left(\frac{d\ln B}{d\ln R}\right)^2 M_A^{-2}\left\{(1-\varepsilon)\left[X(1+3\varepsilon) + 4\chi X\varepsilon + \frac{Y^2}{2}(1-\varepsilon)\right] + (1+\varepsilon)\chi\tilde\kappa^2\left[Y\varepsilon - \frac{X}{4}(1+3\varepsilon)\right]\right\}\\ &+\frac{d\ln B}{d\ln R}\left(\frac{d\ln\Omega^2}{d\ln R}\right)_{MC}M_A^{-2}\left\{\frac{\chi}{2}\tilde\kappa^2(X-Y)\varepsilon(1+\varepsilon) - 2(3\chi-2)\varepsilon(1-\varepsilon) - \frac{\chi}{8}X\left(\frac{d\ln\Omega^2}{d\ln R}\right)_{MC}\varepsilon(7+5\varepsilon)\right.\\ &+\frac{Y^2}{4}\varepsilon^2(1-\varepsilon)^2 + \frac{\chi}{2}X\frac{d\ln B}{d\ln R}(1+3\varepsilon)(1+\varepsilon) + M_A^{-2}\chi Y\left[\frac{1}{4}\frac{d\ln B}{d\ln R}\left(\frac{d\ln\Omega^2}{d\ln R}\right)_{MC}\varepsilon^2(1+3\varepsilon) - 2\varepsilon(1-\varepsilon)\right.\\ &\left.\left.-\frac{1}{8}\left(\frac{d\ln\Omega^2}{d\ln R}\right)^2_{MC}\varepsilon^2(11+3\varepsilon) - \frac{1}{2}\left(\frac{d\ln B}{d\ln R}\right)^2\varepsilon(1+3\varepsilon)\right]\right\} - \left(\frac{d\ln\Omega^2}{d\ln R}\right)^2_{MC}M_A^{-2}\left\{\frac{\chi}{8}Y\tilde\kappa^2\varepsilon(1+3\varepsilon) + \frac{\chi}{2}X\varepsilon\right.\\ &\left[(1-\varepsilon) - \tilde\kappa^2\varepsilon + \left(\frac{d\ln\Omega^2}{d\ln R}\right)_{MC}\varepsilon\right] + \frac{\chi}{4}M_A^{-2}\varepsilon^2\left[\left(\frac{d\ln\Omega^2}{d\ln R}\right)^2_{MC}\varepsilon^2 + 2(1-\varepsilon)\right] - \frac{Y^2}{8}\varepsilon^2(1-\varepsilon)\left.\right\}\\ &+\left[\frac{d\ln\Omega^2}{d\ln R}(1-\varepsilon) + Y(1-\varepsilon)^2 + X(1-\varepsilon)^2\right]\left(\frac{\tilde\kappa^2Y}{4} + X\right) = 0.\end{aligned} \tag{16}$$

Here $s = \omega/\Omega$ is the dimensionless growth rate, $\tilde{\kappa} = \kappa/\Omega$ is the dimensionless epicyclic frequency, X $= (\mathrm{k}\nu_A/\Omega)^2$ where $\nu_A^2 = B^2/4\pi\rho$is the Alfvén velocity, Y $= (\mathrm{k}\nu_H/\Omega)^2$ where $\nu_H^2 = \Omega.\mathbf{B}c/2\pi e\mathrm{n}_e$is the Hall velocity. We define the magnetic field gradient and the velocity gradient produced by the magnetization currents in dimensionless form as G $= d\ \ln\ B\ /\ d\ \ln\ R$ and T $= (d\ \ln\ \Omega^2\ /\ d\ \ln\ R)_{MC}$. Unlike our previous investigation [12], we use the subscript MC to emphasize the additional velocity gradient terms which come from the magnetization currents. If $\mathcal{R}(s) > 0$, the perturbations show an exponential growth with time, and the disc becomes unstable. If $\mathcal{R}(s) < 0$, then the perturbations show an exponential decay with time, and no instability occurs.

3. Growth Rates

Following [12], we solve the dispersion relation given by Eq. (16) for three cases: (i) **Case 1:** $\varepsilon \neq 0, \nabla B = 0$ and $\nabla v_\perp = 0$; (ii) **Case 2:** $\varepsilon \neq 0$, $\nabla B \neq 0$ and $\nabla v_\perp = 0$; (iii) **Case 3:** $\varepsilon \neq 0$, $\nabla B \neq 0$ and $\nabla v_\perp \neq 0$. We investigate the dependence of the growth rates on epicyclic frequencies in each case. In accretion discs, the angular velocity distribution is given by $\Omega(R) \sim R^{-q}$where the shear parameter q can be expressed as

$$q = \frac{d\ln\Omega}{d\ln R}. \tag{17}$$

The epicyclic frequency can be written as a function of the shear parameter by $\kappa^2 = 4\Omega^2 + d\,\Omega^2/d\ \ln\ R \equiv 2\Omega^2\ (2 - q)$. For Keplerian rotation $q = 3/2$, and thus $\kappa^2 = \Omega^2$. The local stability of a disc with a Keplerian rotation profile has been investigated in [12]. Here, we present calculations for $\kappa^2 = 0.5\Omega^2$, $\kappa^2 = \Omega^2$ and $\kappa^2 = 5\Omega^2$ to compare the numerical growth rates of the instability of non-Keplerian cases with those for the Keplerian case. This allows us to see the behaviour of the new unstable regions produced by magnetization effects in various rotation laws. $\kappa^2 = 0.5\Omega^2$ corresponds to the orbits where $q > 3/2$, and $\kappa^2 = 5\Omega^2$ corresponds to an outwardly increasing angular velocity profile.

Case 1: $\varepsilon \neq 0$, $\nabla B = 0$ and $\nabla v_\perp = 0$. First, we ignore the magnetic field and the perpendicular velocity gradients produced by the magnetization current. We note that the dispersion relation for this case is reduced to Eq. (62) of [9] when the magnetization vanishes ($\varepsilon = 0$). Previously, [11] and [12] who extended the analysis of [9] including the magnetization effect, showed that the unstable regions widen with increasing magnetization, i.e. ε value. Here, we keep the magnetization constant ($\varepsilon = 0.5$), and change the rotation law.

The growth rate of the classical MRI is proportional to q[19]. The epicyclic frequency provides a measure of stabilization as the epicyclic motions generated by Coriolis forces effectively stabilize both linear and nonlinear perturbations. The stabilization of the flow can be achieved by increasing the epicyclic frequency through decreasing the value of q from 2 [20]. If q value approaches 2, then κ^2 approaches 0. As a result, the dynamical stabilization weakens. We apparently see this effect in Figure 1. We present our solutions for the epicyclic frequencies $\kappa^2 = 0.5\Omega^2$, $\kappa^2 = \Omega^2$ and $\kappa^2 = 5\Omega^2$. Figure 1 shows the graphical solutions in the XY plane. The mounds represent the regions of instability. The maximum growth rate which is found as $\mathrm{s}_m = 0.88$ is highest when $\kappa^2 = 0.5\Omega^2$. The solution for $\kappa^2 = \Omega^2$ with a maximum growth rate $\mathrm{s}_m = 0.75$ corresponds to the Keplerian rotation, and thus to the solution in [12] (see Figure 3b therein). Bottom panel of Figure 1 corresponds to a disc with an outwardly increasing velocity profile, i.e. $d\Omega^2/dR > 0$. We see the region of instability becomes much narrower and only the regions where $Y < 0$ are unstable in this case. Y < 0 describes the configuration where Ω and $\boldsymbol{B}$ are oriented in the opposite direction, i.e. $\Omega \cdot \boldsymbol{B} < 0$.

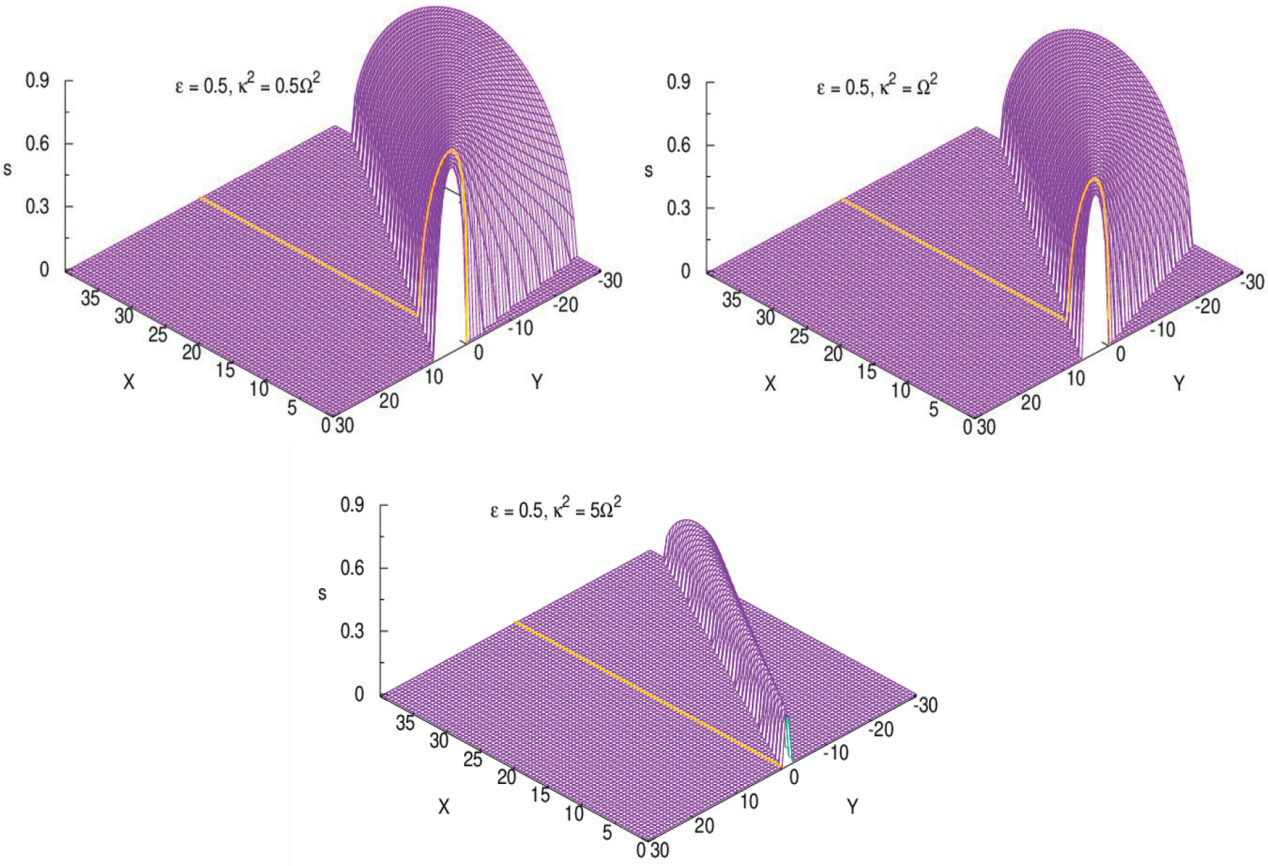

Figure 1. Growth rates for Case 1 where $\nabla B = 0$ and $\nabla v_{\perp} = 0$ for $\kappa^2 = 0.5\Omega^2$ (*top left*), $\kappa^2 = \Omega^2$ (*top right*) and $\kappa^2 = 5\Omega^2$ (*bottom*). The mounds correspond to the regions of instability and the height of these mounds are proportional to the dimensionless growth rate. We use the same scaling for the s-axis to allow for direct comparison of the growth rates for each solution. Growth rate for the ideal MHD case (Y = 0) is represented with the yellow line in each plot.

In Figure 1, we also show where the ideal MHD case (where $Y = 0$) is located in order to compare with the non-ideal case. The yellow line shows the growth rate found in the ideal MHD limit. The role of the Hall effect on the development of MRI was first examined by [21]. [21] found that the inclusion of the Hall currents modify the growth rates of the instability depending on the initial field being parallel ($\Omega \cdot \mathbf{B} > 0$) or antiparallel ($\Omega \cdot \mathbf{B} < 0$) to the disc rotation axis. Furthermore, [9] showed that no instability occurs in an outwardly increasing velocity profile without the Hall effect. This result is recovered in the bottom panel of Figure 1, as it should. The maximum growth rate values for $\kappa^2 = 0.5\Omega^2$ and $\kappa^2 = \Omega^2$ remains unchanged from the ideal limit (see also [9, 21]).

We also note that our top right and bottom panels of Figure 1 are reduced to Figures 5 and 6 of [9] when $\varepsilon = 0$. We present the solutions with and without magnetization in Figure 2 with color maps in order to enable direct comparison between the wavelength ranges of the unstable mode. When compared with results of [9], we see that the region of instability in the XY parameter space becomes slightly wider with the inclusion of magnetization. Our solutions, however, have the same maximum growth rate as found in [9] with $s_m = 0.75$ for $\kappa^2 = \Omega^2$ and $s_m = 0.25$ for $\kappa^2 = 5\Omega^2$.

Thus, the inclusion of magnetization only, does not change the behaviour of the region where the instability occurs depending on epicyclic frequency. We shall see this behaviour is qualitatively different when

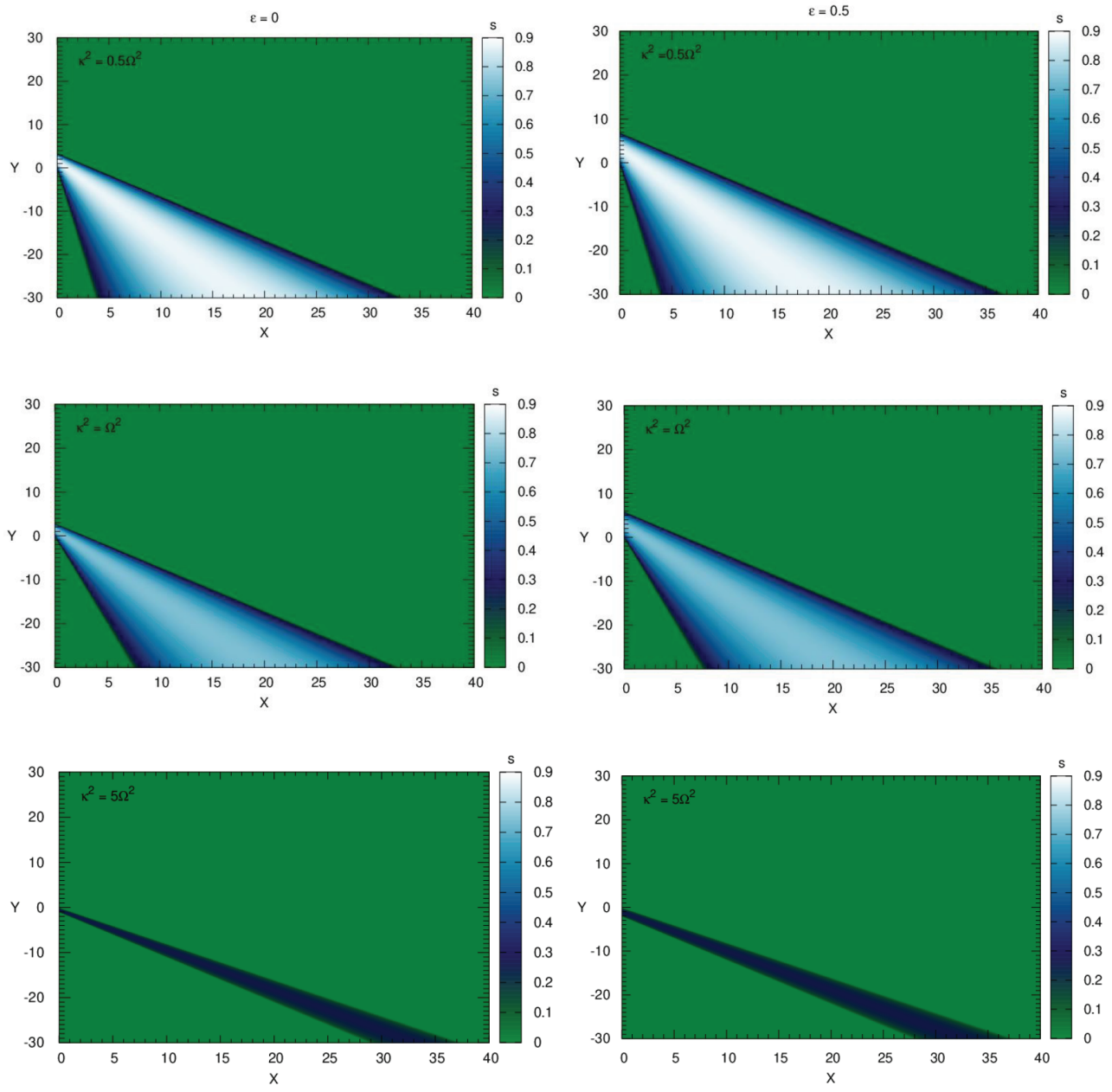

Figure 2. Color maps showing the comparison of the growth rates obtained when the magnetization is ignored, i.e. $\varepsilon = 0$ (*left panel*) and included, i.e. $\varepsilon = 0.5$ (*right panel*) for $\kappa^2 = 0.5\Omega^2$ (*top*), $\kappa^2 = \Omega^2$ (*middle*) and $\kappa^2 = 5\Omega^2$ (*bottom*). The left panel corresponds to the results of [9]. When the magnetization is included, the ridges become slightly wider. The maximum growth rates, however, remains unchanged.

the magnetic field gradient is included.

Case 2: $\varepsilon \neq 0$, $\nabla B \neq 0$ and $\nabla v_\perp = 0$. Here, we consider the case where the charged particles create a magnetization current which is persistent enough to create a gradient in the magnetic field. Previously, it has already been shown that the inclusion of the magnetic field gradient (both radial and azimuthal) produces an another unstable region in the XY plane for the Keplerian case [11 – 12, 22]. We call the ridge found from the classical MRI analyses with HEMFs as *the unstable region – I* (UR-I) and the second unstable region produced

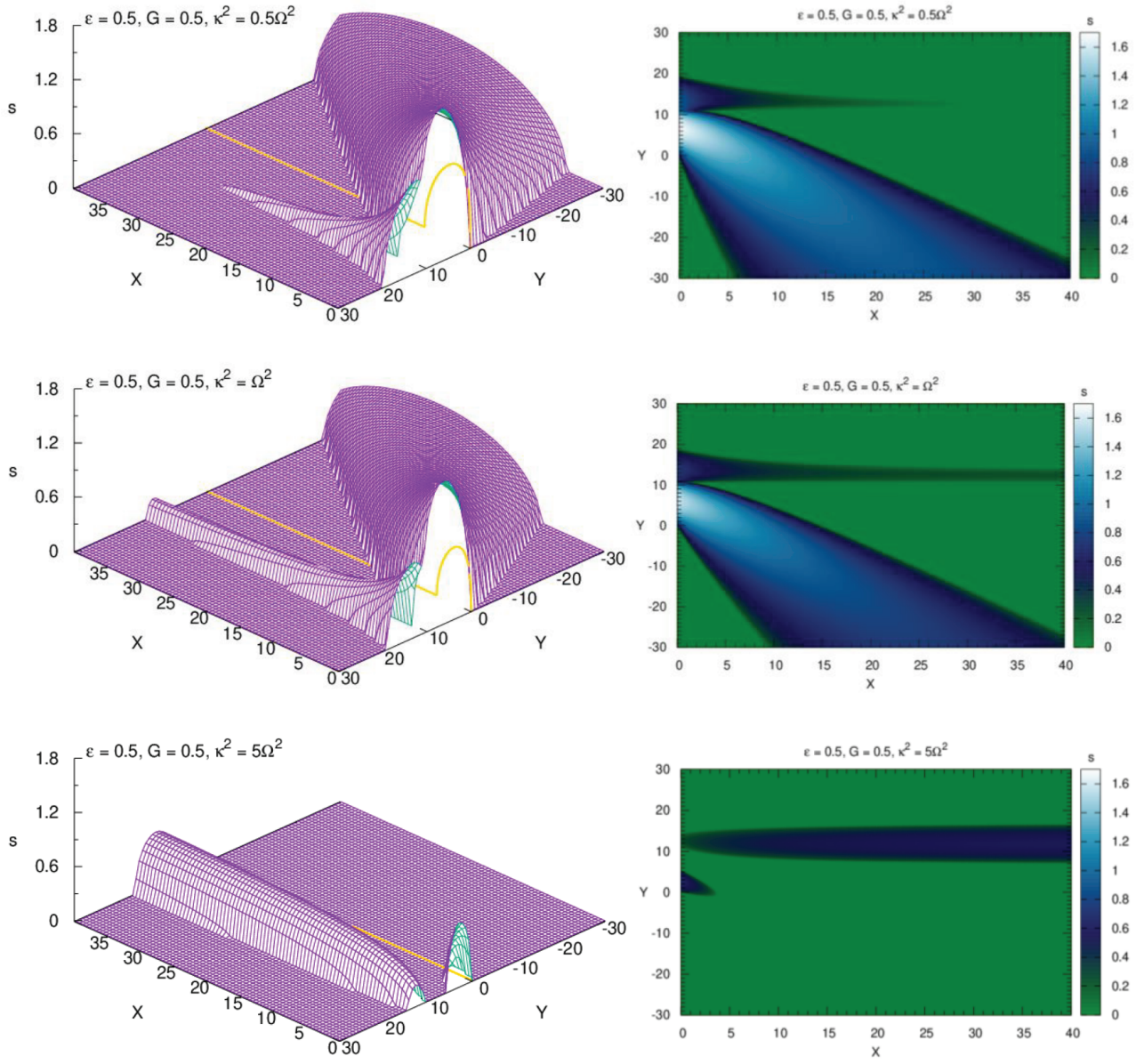

Figure 3. Growth rates for Case 2 where $\nabla B \neq 0$ and $\nabla v_{\perp} = 0$ for $\kappa^2 = 0.5\Omega^2$ (*top left*), $\kappa^2 = \Omega^2$ and $\kappa^2 = 5\Omega^2$ (*bottom*). *Left panel* shows the three-dimensional plot of the growth rates and *the right panel* shows the corresponding colormaps which show the growth rates in the XY plane. The UR-I almost vanishes when $d\Omega^2/dR > 0$. But the UR-II which is produced when the magnetic field gradient is included still exists. Growth rate for the ideal MHD case (Y = 0) is represented with the yellow line in each plot in the *left panel*.

when the magnetic field gradient is included as *the unstable region – II* (UR-II). Figure 3 shows the solutions for Case 2 both in three-dimensional plots and in color maps. In Figure 3, we see that the UR-I again becomes narrower with the increase in the epicyclic frequency. Furthermore, this unstable region nearly vanishes when $\kappa^2 = 5\Omega^2$. The maximum growth rate for UR-I is $s_m = 1.68$ for $\kappa^2 = 0.5\Omega^2$, and $s_m = 0.69$ for $\kappa^2 = 5\Omega^2$. On the other hand, UR-II becomes wider and spreads over a larger space in the XY plane than UR-I does when $\kappa^2 = 5\Omega^2$. The maximum growth rate for UR-II is $s_m = 1.01$ for $\kappa^2 = 0.5\Omega^2$, and $s_m = 0.6$ for $\kappa^2 = 5\Omega^2$.

With the inclusion of the magnetic field gradient, the wavenumber range where the instability occurs, shifts to the Y $>$ 0 region in the outwardly increasing velocity profile. Figure 3 shows that the departure from the ideal limit is remarkable when the Hall term and the magnetization are both introduced.

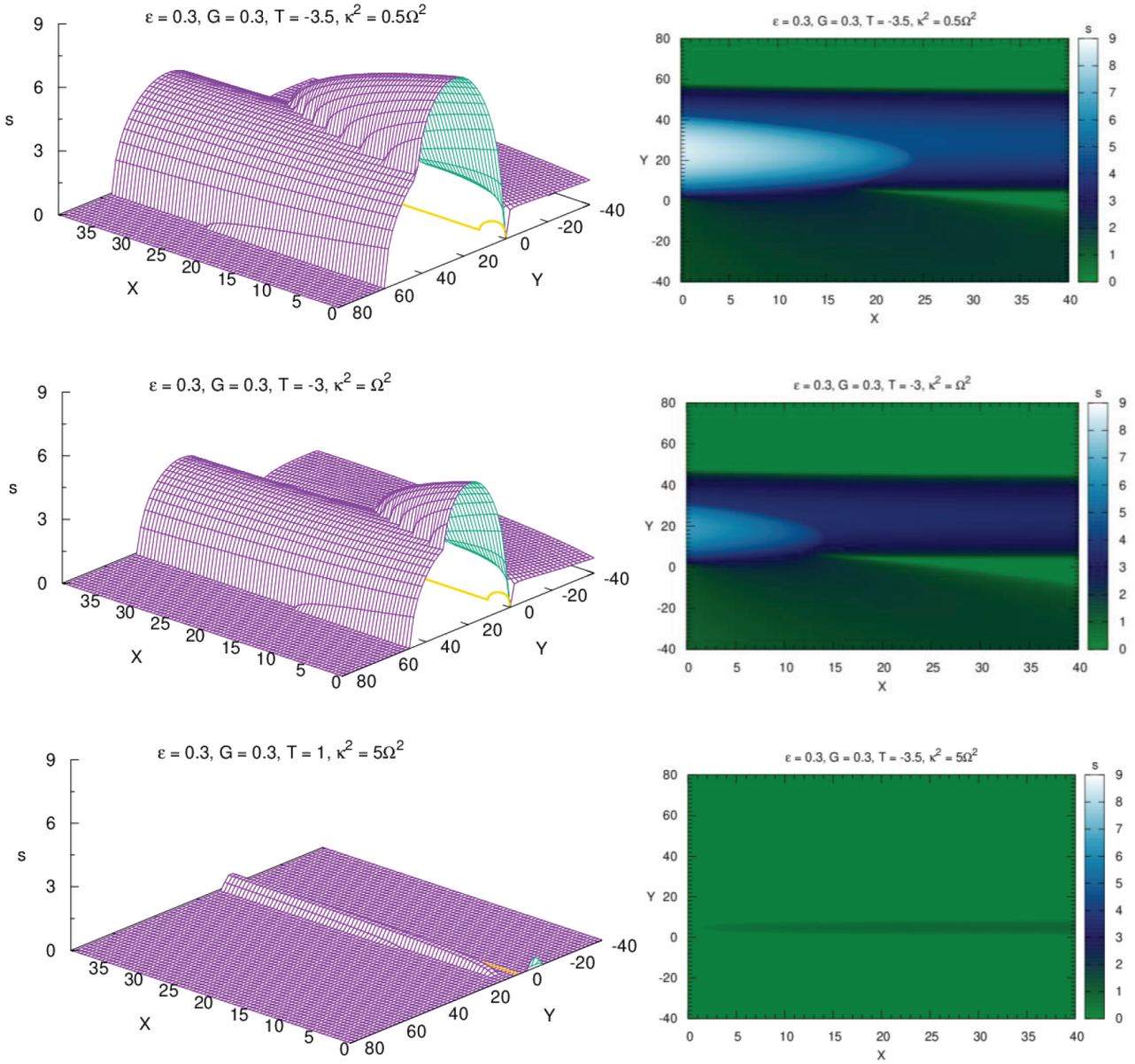

Figure 4. Growth rates for Case 3 where we assume $\nabla B \neq 0$ and $\nabla v_{\perp} \neq 0$ for $\kappa^2 = 0.5\Omega^2$ (*top*), $\kappa^2 = \Omega^2$ (*middle*) and $\kappa^2 = 5\Omega^2$ (*bottom*). *Left panel* shows the three-dimensional plot of the growth rates and *the right panel* shows the corresponding colormaps which show the growth rates in the XY plane for Case 3. T and κ^2 values are related to each other by definition of epicyclic frequency. The UR-I vanishes in an outwardly increasing velocity profile. The UR-II still exists in a narrow region with a maximum growth rate $s_m = 0.59$.

Case 3: $\varepsilon \neq 0$, $\nabla B \neq 0$ and $\nabla v_{\perp} \neq 0$. The graphical solutions for this case are shown in Figure 4. As expected, the growth rates are higher and the unstable wavenumber range is larger for $\kappa^2 = 0.5\Omega^2$ than those for the Keplerian case. The maximum growth rate is $s_m = 8.58$ for $\kappa^2 = 0.5\Omega^2$, and $s_m = 6.65$ for $\kappa^2 = \Omega^2$.

The growth rates become much lower when $d\Omega^2/dR > 0$. We see that the UR-I vanishes in this case. However, the UR-II produced by the diamagnetic effect still exists. The maximum growth rate of this new unstable region is $s_m = 0.59$. In the classical HEMF MRI where the diamagnetic effects are ignored, this value has been found as 0.25 [9]. As a result, whatever the epicyclic frequency value is, decreasing the magnetic field strength which is already weak, leads to more rapid growth of instability.

4. Conclusion

The effects of diamagnetism on MRI have previously been investigated by [11] and [12] for Keplerian discs. In this paper, we generalized these analyses for discs/regions of the discs where the rotation profile is non-Keplerian. Our results show that the magnetic field and the velocity gradients produced by the magnetization currents play an important role in triggering the MRI both for an increasing and for a decreasing angular momentum with radius. The second unstable region produced by magnetization effects still exists even if $d\Omega^2/dR > 0$. Moreover, the UR-II becomes more dominant than UR-I in XY parameter space. Whatever the epicyclic frequency value is, the second unstable region always appears in $Y > 0$ region. Inclusion of the diamagnetic effects increases the maximum dimensionless growth rate from $s_m = 0.25$ which has been found from the classical HEMF MRI analysis to $s_m = 0.59$ for an outwardly increasing velocity profile. This result shows the importance of the diamagnetic effect on instability. Regions in which the angular velocity increases outwards are normally stable in the standart MRI. Inclusion of the Hall effect allows instability to occur in these regions, and diamagnetism makes the instability more powerful. The behaviour discussed in this paper is relevant to astrophysical discs in a variety of systems where the epicyclic frequency deviates from Keplerian profile. There are several circumstances where $q > 3/2$ and thus $\kappa^2 \to 0$, especially in the inner regions of accretion discs around black holes due to the relativistic effects, and in the outer (inner) regions of the circumprimary (circumbinary) discs in binary systems due to tidal torques. The regime in which the angular velocity increases outwards might be relevant to the boundary layer between a star and a disc (see also [23]). The velocity distribution might also change locally if the velocity gradient produced by the magnetization current is persistent. Thus, the diamagnetic effect itself may lead to a deviation from the Keplerian rotation.

In conclusion, diamagnetism has a strong destabilizing role in any rotation profile. Decreasing the magnetic field strength which is already weak, leads to more rapid growth of instability both for $0 < \kappa^2 < \Omega^2$ and for $\kappa^2 > 4\Omega^2$.

Acknowledgement

I would like to thank the anonymous referees for their constructive suggestions that improved the manuscript. This study is partly supported by the Turkish Scientific and Technical Research Council (TÜBİTAK-117F280).

References

[1] Velikhov EP. Stability of an ideally conducting liquid flowing between cylinders rotating in a magnetic field. Journal of Experimental and Theoretical Physics 1959; 36 (9), 5: 1398-1404.

[2] Chandrasekhar S. The stability of non-dissipative couette flow in hydromagnetics. Proceedings of the National Academy of Sciences of the United States of America 1960; 46 (2): 253-257. doi: 10.1073/pnas.46.2.253

[3] Balbus SA, Hawley JF. A powerful local shear instability in weakly magnetized disks. I - Linear analysis. II - Nonlinear evolution. The Astrophysical Journal 1991; 376: 214-233. doi: 10.1086/170271

[4] Hawley JF, Gammie CF, Balbus SA. Local three-dimensional magnetohydrodynamic simulations of accretion disks. The Astrophysical Journal 1995; 440: 742-763. doi: 10.1086/175311

[5] Brandenburg A, Nordlund A, Stein RF, Torkelsson U. Dynamo-generated turbulence and large-scale magnetic fields in a keplerian shear flow. The Astrophysical Journal 1995; 446: 741-754. doi: 10.1086/175831

[6] Balbus SA, Hawley JF, Stone JM. Nonlinear stability, hydrodynamical turbulence, and transport in disks. The Astrophysical Journal 1996; 467: 76–86. doi: 10.1086/177585

[7] Hawley JF, Richers SA, Guan X, Krolik JH. Testing convergence for global accretion disks. The Astrophysical Journal 2013; 772 (2): 102–119. doi: 10.1088/0004-637X/772/2/102

[8] Balbus SA, Hawley JF. Instability, turbulence, and enhanced transport in accretion disks. Reviews of Modern Physics 1998; 70: 1-53. doi: 10.1103/RevModPhys.70.1

[9] Balbus SA, Terquem C. Linear Analysis of the Hall Effect in Protostellar Disks. The Astrophysical Journal 2001; 552: 235-247. doi: 10.1086/320452

[10] Shakura N, Postnov K. On properties of Velikhov-Chandrasekhar MRI in ideal and non-ideal plasma. Monthly Notices of the Royal Astronomical Society 2015; 448 (4): 3697-3706. doi: 10.1093/mnras/stu2560

[11] Devlen E, Pekünlü ER. Influence of the diamagnetic effect on the magnetorotational instability in accretion discs. Monthly Notices of the Royal Astronomical Society 2007; 377: 1245-1262. doi: 10.1111/j.1365-2966.2007.11677.x

[12] Doğan S, Pekünlü ER. MRI: A possible mechanism for funnel flows?. Publications of the Astronomical Society of Australia 2012; 124 (919): 922-933. doi: 10.1086/667974

[13] Abramowicz M, Brandenburg A, and Lasota JP. The dependence of the viscosity in accretion discs on the shear/vorticity ratio. Monthly Notices of the Royal Astronomical Society 1996; 281: L21-L24. doi: 10.1093/mnras/281.2.L21

[14] Lubow SH, Ogilvie GI. On the tilting of protostellar disks by resonant tidal effects. The Astrophysical Journal 2000; 538: 326-340. doi: 10.1086/309101

[15] Facchini S, Lodato G, Price DJ. Wave-like warp propagation in circumbinary discs - I. Analytic theory and numerical simulations. Monthly Notices of the Royal Astronomical Society 2013; 433: 2142-2156. doi: 10.1093/mnras/stt877

[16] Frank J, King AR, Raine DJ. Accretion Power in Astrophysics: Third Edition, Cambridge Univ. Press, Cambridge, 2002.

[17] Singal AK. Magnetization effects in an incoherent synchrotron source. Astronomy and Astrophysics 1986; 155: 242-246.

[18] Bodo G, Ghisellini G, Trussoni E. Diamagnetic effects in synchrotron sources. Monthly Notices of the Royal Astronomical Society 1992; 255: 694-700. doi: 10.1093/mnras/281.2.L21

[19] Balbus SA, Hawley JF. A powerful local shear instability in weakly magnetized disks. IV. Nonaxisymmetric perturbations. The Astrophysical Journal 1992; 400: 610-621. doi: 10.1086/172022

[20] Hawley JF, Balbus SA, Winters WF. Local hydrodynamic stability of accretion disks. The Astrophysical Journal 1999; 518 (1): 394-404. doi: 10.1086/307282

[21] Wardle M. The Balbus – Hawley instability in weakly ionized discs. Monthly Notices of the Royal Astronomical Society 1999; 307: 849-856. doi: 10.1046/j.1365-8711.1999.02670.x

[22] Doğan S. Magnetic field gradient effects on the magnetorotational instability. Astronomische Nachrichten 2017; 338: 740-747. doi: 10.1002/asna.201713275

[23] Ogilvie GI. On the dynamics of magnetorotational turbulent stresses, Monthly Notices of the Royal Astronomical Society 2003; 340: 969–982. doi: 10.1046/j.1365-8711.2003.06359.x